

# High-throughput automated organoid culture via stem-cell aggregation in microcavity arrays

Nathalie Brandenburg<sup>1,6,8</sup>, Sylke Hoehnel<sup>1,6,8</sup>, Fabien Kuttler<sup>2,8</sup>, Krisztian Homicsko<sup>3</sup>,  
Camilla Ceroni<sup>1,6</sup>, Till Ringel<sup>4</sup>, Nikolce Gjorevski<sup>1,7</sup>, Gerald Schwank<sup>4</sup>, George Coukos<sup>3</sup>,  
Gerardo Turcatti<sup>2</sup> and Matthias P. Lutolf<sup>1,5</sup> ✉

**Stem-cell-derived epithelial organoids are routinely used for the biological and biomedical modelling of tissues. However, the complexity, lack of standardization and quality control of stem cell culture in solid extracellular matrices hampers the routine use of the organoids at the industrial scale. Here, we report the fabrication of microengineered cell culture devices and scalable and automated methods for suspension culture and real-time analysis of thousands of individual gastrointestinal organoids trapped in microcavity arrays within a polymer-hydrogel substrate. The absence of a solid matrix substantially reduces organoid heterogeneity, which we show for mouse and human gastrointestinal organoids. We use the devices to screen for anticancer drug candidates with patient-derived colorectal cancer organoids, and apply high-content image-based phenotypic analyses to reveal insights into mechanisms of drug action. The scalable organoid-culture technology should facilitate the use of organoids in drug development and diagnostics.**

Gastrointestinal (GI) organoids have emerged as unique *in vitro* models for studying organ development, function and disease<sup>1,2</sup>. However, owing to the difficulty of standardizing existing methods, the organoid technology has not yet been widely adopted in pharmaceutical drug development or diagnostics<sup>3,4</sup>. In particular, the necessity to grow organoids in drops of solidified Matrigel<sup>5,6</sup> renders the development of reliable assays cumbersome, as local differences in physical parameters and growth factor accessibility cause variability in shape, size and distribution of organoids<sup>7,8</sup>. Furthermore, as individual three-dimensionally (3D) grown organoids are located at different focal planes, it remains a challenge to extract quantitative data from such imaging experiments.

Pioneering attempts to improve GI organoid culture for screening assays have focused on deriving organoids on poly(styrene)-coated poly(dimethylsiloxane) (PDMS) microwell substrates<sup>9</sup> or on flat layers of Matrigel<sup>10–13</sup>. The former approach is well suited for high-throughput clonogenic culture and the subsequent retrieval of individual organoids, for example, for downstream analyses using quantitative PCR<sup>9</sup>, but the reliance on a non-physiological polymer substrate compromises organoid development and, therefore, limits its broader applicability. The culture of organoids on flat Matrigel films<sup>10</sup>, in some cases sandwiched with another layer of Matrigel<sup>11–13</sup>, enables the generation of organoid arrays, as well as their imaging and tracking over time. However, this approach has a relatively poor throughput (around 4 organoids per mm<sup>2</sup>) and reproducibility because organoids develop randomly, similar to the classical 3D-culture setting<sup>5,6</sup>. Thus, although early efforts to improve organoid culture have demonstrated some promise, issues of limited scalability, lack of robustness of morphogenesis and incompatibility with high-content phenotypic analyses remain to be tackled.

Here, to address these shortcomings, we introduce a technology for the high-throughput derivation of epithelial organoids from defined stem cell (SC) aggregates in a solid matrix-free manner. Specifically, we developed microengineered hydrogel films on the bottom of conventional multiwell plates to simultaneously derive thousands of uniform organoids at predefined locations on the same focal plane. The precise control of the starting SC population was found to be a critical parameter for improving the robustness of *in vitro* organogenesis and the homogeneity of the final tissues, far exceeding what can be achieved using conventional 3D cultures. A proof-of-concept anticancer drug screening on patient-derived colorectal cancer (CRC) organoids demonstrated the potential of our approach for automated organoid derivation and high-content phenotypic drug testing. This technology provides exciting perspectives for the standardization of organoid-based assays for drug discovery and diagnostics.

## Results

**Development of the organoid array technology.** A cornerstone of our approach is a microengineered hydrogel substrate that comprises an array of regularly spaced, round-bottom microcavities (Fig. 1) and that was conceived on the basis of three main design criteria: (1) at the onset of an organoid culture, individual microcavities should promote fast aggregation of epithelial (stem) cells, which we reasoned would be a crucial step for establishing homogeneously sized and polarized epithelial tissues as a starting material for *in vitro* organogenesis; (2) individual microcavities should act as stable traps for organoids and, therefore, contribute to their efficient partitioning into a regular organoid array; (3) through the provision of geometrical and microenvironmental signals, the microcavities

<sup>1</sup>Laboratory of Stem Cell Bioengineering, Institute of Bioengineering, School of Life Sciences, EPFL, Lausanne, Switzerland. <sup>2</sup>Biomolecular Screening Facility, School of Life Sciences, EPFL, Lausanne, Switzerland. <sup>3</sup>Department of Oncology, University Hospital of Lausanne, and Lausanne Branch, Ludwig Institute for Cancer Research, University of Lausanne, Lausanne, Switzerland. <sup>4</sup>Institute of Molecular Health Sciences, ETH Zurich, HPL, Zürich, Switzerland. <sup>5</sup>Institute of Chemical Sciences and Engineering, School of Basic Sciences, EPFL, Lausanne, Switzerland. <sup>6</sup>Present address: Startlab/SUN bioscience, Bâtiment SE-B, Biopôle, Epalignes, Switzerland. <sup>7</sup>Present address: Roche Pharma Research and Early Development, Basel, Switzerland. <sup>8</sup>These authors contributed equally: Nathalie Brandenburg, Sylke Hoehnel, Fabien Kuttler. ✉e-mail: [matthias.lutolf@epfl.ch](mailto:matthias.lutolf@epfl.ch)

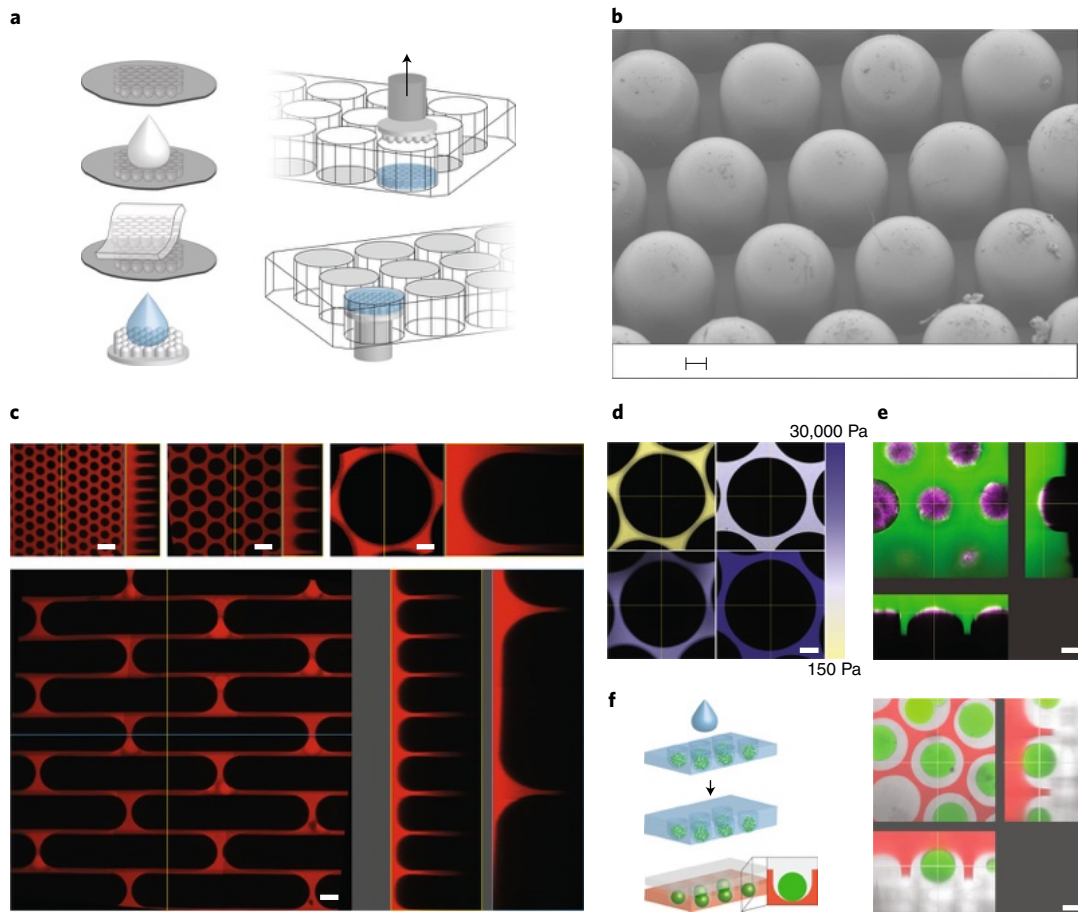


**Fig. 1 | Organoid array technology.** **a**, Schematic of the fabrication of the hydrogel-based U-shaped microwell arrays. U-shaped microcavities were generated on silicon substrates using standard Si Bosch processes and soft lithography. A PDMS mould was then generated by counter-moulding the silicon substrate. Finally, the microcavities were imprinted onto hydrogel surfaces (blue) during the hydrogel cross-linking. **b**, SEM image of the PDMS stamp containing round pillars (diameter, 100  $\mu\text{m}$ ). Scale bar, 20  $\mu\text{m}$ ; original magnification,  $\times 250$ . **c**, Confocal microscopy images of PEG hydrogel arrays of 50  $\mu\text{m}$ , 100  $\mu\text{m}$  and 500  $\mu\text{m}$  in diameter and rod-shaped microcavities. The top and the side views are shown. Scale bars, 100  $\mu\text{m}$ . **d**, Colour-coded confocal representation of the range of stiffness that our microwell arrays can have—from 150 Pa (yellow) to 30,000 Pa (purple). Scale bar, 100  $\mu\text{m}$ . **e**, Confocal microscopy images of the functionalization of the U-shaped microwell arrays. Green fluorescently labelled PEG was used to represent the gel. The bottom of each microwell is functionalized with fluorescently labelled bovine serum albumin (magenta). Scale bar, 100  $\mu\text{m}$ . **f**, Perspective illustration of 3D encapsulated PEG hydrogel microbeads by sandwich-casting a second layer of substrate, showing the potential to combine the localization of organoids in one single z plane in combination with 3D cultures (left). Right, confocal microscopy images of the sandwich-casting approach. An array of microwells (diameter, 400  $\mu\text{m}$ ) is shown in red fluorescently labelled PEG hydrogel substrate (elastic modulus  $G'$ , 12.5 kPa). The top matrix consists of far-red fluorescently labelled PEG hydrogel substrate ( $G'$ , 12.5 kPa) encasing green fluorescent PEG microbeads (diameter,  $\sim 200 \mu\text{m}$ ). Scale bars, 100  $\mu\text{m}$ .

should act as artificial niches to direct the development of epithelial SC aggregates into organoids.

We used soft-lithography-based methods in combination with replica moulding<sup>14</sup> to fabricate hydrogel microcavity arrays directly onto the surface of conventional plastic or glass cell culture ware (Fig. 1a). This approach is compatible with a wide range of hydrogels, including those that are cross-linked from naturally derived macromolecules (Supplementary Fig. 1). Here we focused on poly(ethylene glycol) (PEG)-based hydrogels because of their advantageous optical and non-fouling properties, as well as their exquisite modularity for tuning both the physical and biochemical properties of the material<sup>15</sup>. Scanning electron microscopy (SEM) analysis demonstrated that PEG hydrogel films can be readily moulded into arrays of perfectly U-shaped microcavities (Fig. 1b). Importantly, the diameter, depth and spacing of microcavities can be freely chosen (Fig. 1c) such as to accommodate developing tissues of different size and complexity. Furthermore, by varying the concentration of

PEG prepolymer, we can precisely tune the stiffness of the hydrogel substrate across a relatively wide range (30–150 kDa), and without introducing any distortion of the microstructure features (Fig. 1d). Finally, the biochemical nature of the hydrogel substrates can be tailor-made by conjugating desirable bioactive ligands to the otherwise inert gel network, or by filling the microcavities with natural or synthetic matrices (Fig. 1e,f) such as to embed trapped tissues in 3D.

**Technology validation using mouse intestinal organoids.** We first used *Lgr5*-eGFP<sup>+</sup> mouse intestinal SCs (ISCs) to test and implement this concept. On the basis of an average maximum size of intestinal organoids of approximately 300  $\mu\text{m}$  in diameter, we chose 400  $\mu\text{m}$  microcavities to generate mouse mini-gut arrays (Fig. 2a). ISCs were seeded on hydrogel microcavity arrays at an average density of 100 cells per microcavity in ENR-CV expansion medium<sup>16</sup> containing soluble Matrigel (2% v/w)<sup>17</sup>. Within 30 min, cells sediment

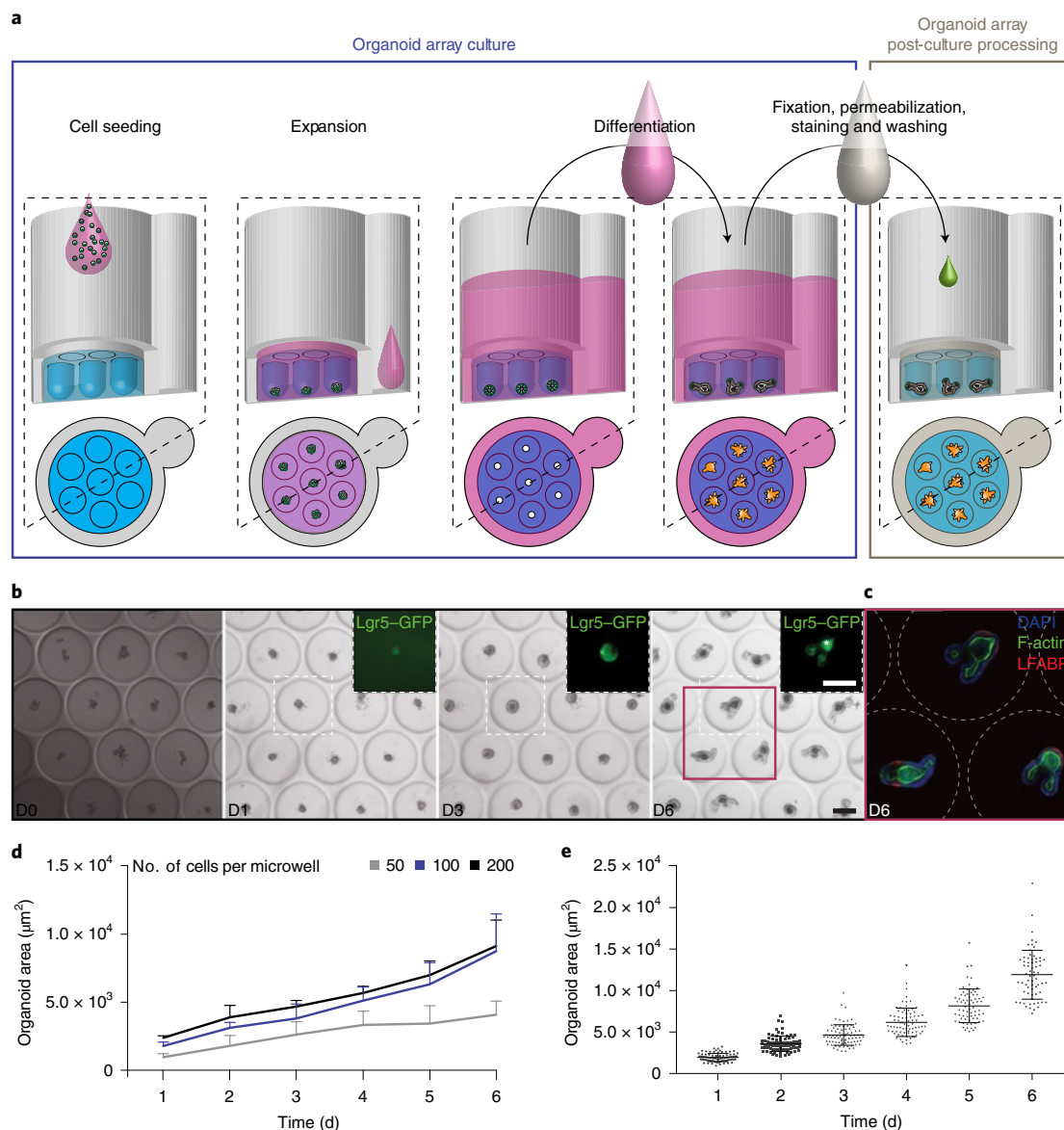


**Fig. 2 | GI organoid array cultures.** **a**, Schematic of intestinal organoids formation from single cells in U-shaped microwell arrays. Single cells are seeded on top of the microwells in SC expansion medium containing 2% Matrigel and left to sediment. The cells aggregate and form luminal SC colonies overnight. These are expanded for a further 2 d and differentiated until day 6. Finally, the organoids are left on the culture substrate and post-processed for further analysis. **b**, Real-time wide-field microscopy images displaying intestinal organoids grown on array at days (D) 0, 1, 3 and 6. The white dotted square shows a magnification of a specific organoid within the array and its expression level of LGR5 over time (green). Scale bars (main image and inset), 200  $\mu\text{m}$ . **c**, The red square shows the expression level of L-FABP in the enterocyte fraction of a specific region of the same array. Scale bar, 200  $\mu\text{m}$ . **d**, Time-course quantification of the area of organoids formed from 50, 100 and 200 fluorescence-activated cell sorting (FACS)-sorted Lgr5<sup>+</sup> ISCs per microwell, averaged from three independent experiments. **e**, Area variability over time for experiments starting from 100 cells per microwell. One representative experiment is shown.

by gravity into individual microcavities, forming compact, albeit irregularly shaped, SC colonies. Within the first 24 h, these ISC aggregates become smooth and form apicobasally (AP)-polarized columnar epithelial tissues (Supplementary Video 1). After switching the medium to differentiation conditions (ENR)<sup>16</sup> at 60 h, crypt-villi morphogenesis is triggered, resulting in the generation of an array of mini-guts that bear one or more crypt-like buds (Fig. 2b, Supplementary Video 2).

Owing to the confinement of individual organoids in their respective microcavity, we can reliably track and quantitatively probe, at the single-organoid level and in high-throughput, the progression from a cellular aggregate to a fully developed organoid,

allocating specific cell identities using immunocytochemistry and fluorescence microscopy. As expected, during the initial SC expansion phase, AP-polarized epithelial tissues are composed of eGFP<sup>+</sup> SCs that are restricted to the buds after induction of differentiation (Fig. 2b, magnification). Subsequent immunostaining, which was performed in our arrays without manual manipulation of the organoids, revealed the presence of all of the major differentiated epithelial cell types of the mouse small intestine—namely enterocytes, Paneth cells, enteroendocrine cells and goblet cells (Fig. 2c, Supplementary Fig. 2a–d). Notably, about  $92 \pm 4\%$  ( $n=3$  independent experiments) of all cell aggregates developed into lumenized mini-guts.

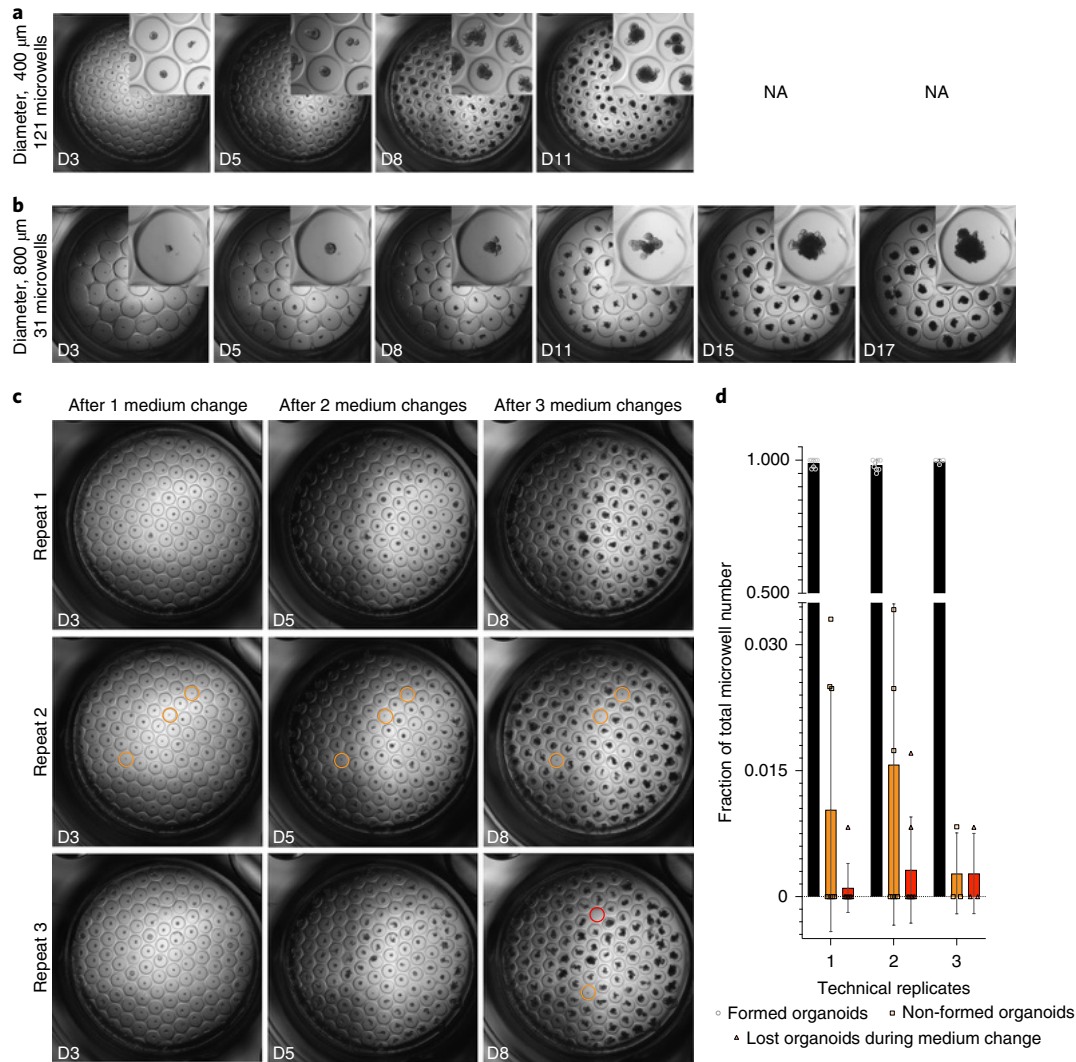


**Fig. 3 | Organoid arrays robustness.** **a,b**, Representative examples of mouse intestinal organoids that were grown for 17 d in microcavities of 400  $\mu\text{m}$  in diameter, in which organoids survive for 8 d before showing signs of substantial organoid death (**a**) or 800  $\mu\text{m}$  in diameter in which organoids can be kept for up to 15 d before showing signs of substantial organoid death (**b**) NA, not available due to organoid death after D11. **c**, Representative examples of non-forming organoids and organoid loss due to repeated medium changes. **d**, Quantification of organoid-formation efficiency. Non-formed organoids and lost organoids due to medium changes account on average for less than 5% of the total amount of microcavities. Data are mean  $\pm$  s.d. Technical replicates 1, 2 and 3 comprised  $n=8$ ,  $n=8$  and  $n=3$  biological replicates, respectively.

We next tested the effect of initial cell aggregate size on organoid formation efficiency and size. For this purpose, we seeded mouse ISCs at an average density of 10, 50, 100 and 200 cells per microcavity on our microstructured hydrogel substrates. Interestingly, whereas we found that 100 and 200 cells gave rise to a similar growth pattern, aggregates that comprised 50 cells or less initially formed AP-polarized SC colonies but were unable to undergo subsequent budding (Fig. 2d). Moreover, aggregates composed of 10 cells showed poor cell survival and failed to generate epithelial structures (data not shown). Notably, by tracing all individual organoids of an array ( $n=121$ , 24-well plate) over 6 d, we can readily measure the size distribution of an organoid population as a function of culture time. SC colonies show a very narrow size distribution (days 1, 2 and 3), which becomes increasingly broader from day 4 onwards, corresponding to the initiation of budding after induction of differentiation (Fig. 2e). These data show that the initial cell number is a critical parameter in the development of organoid cultures and organoid-based assays using our approach.

We also show that the microcavity diameter, together with the density of microcavities per surface unit, directly influences the lifetime of intestinal organoids. We observed that organoids, which were grown in arrays harbouring 121 microcavities of a diameter of 400  $\mu\text{m}$  and in 200  $\mu\text{l}$  medium (replenished every 2 d), could be maintained for a maximum of 8 d (Fig. 3a), whereas the organoids could be maintained for twice as long in arrays harbouring 31 microcavities with 800  $\mu\text{m}$  diameter (Fig. 3b). Importantly, the trapping of organoids in microcavities is very reliable, over extended periods of time and repeated pipetting events—less than 0.5% of all organoids were lost after 10 medium changes (Fig. 3c,d).

In an attempt to replace soluble Matrigel with a more defined extracellular-matrix (ECM) formulation, we investigated whether the key extracellular-matrix components of Matrigel, laminin-111 and collagen type IV, could promote colony formation and organoid morphogenesis. As Matrigel is composed of  $\sim 56\%$  laminin-111 and  $\sim 31\%$  Collagen IV<sup>18</sup>, we deduced that an approximate final concentration of 150  $\mu\text{gml}^{-1}$  of laminin-111 and 80  $\mu\text{gml}^{-1}$  of

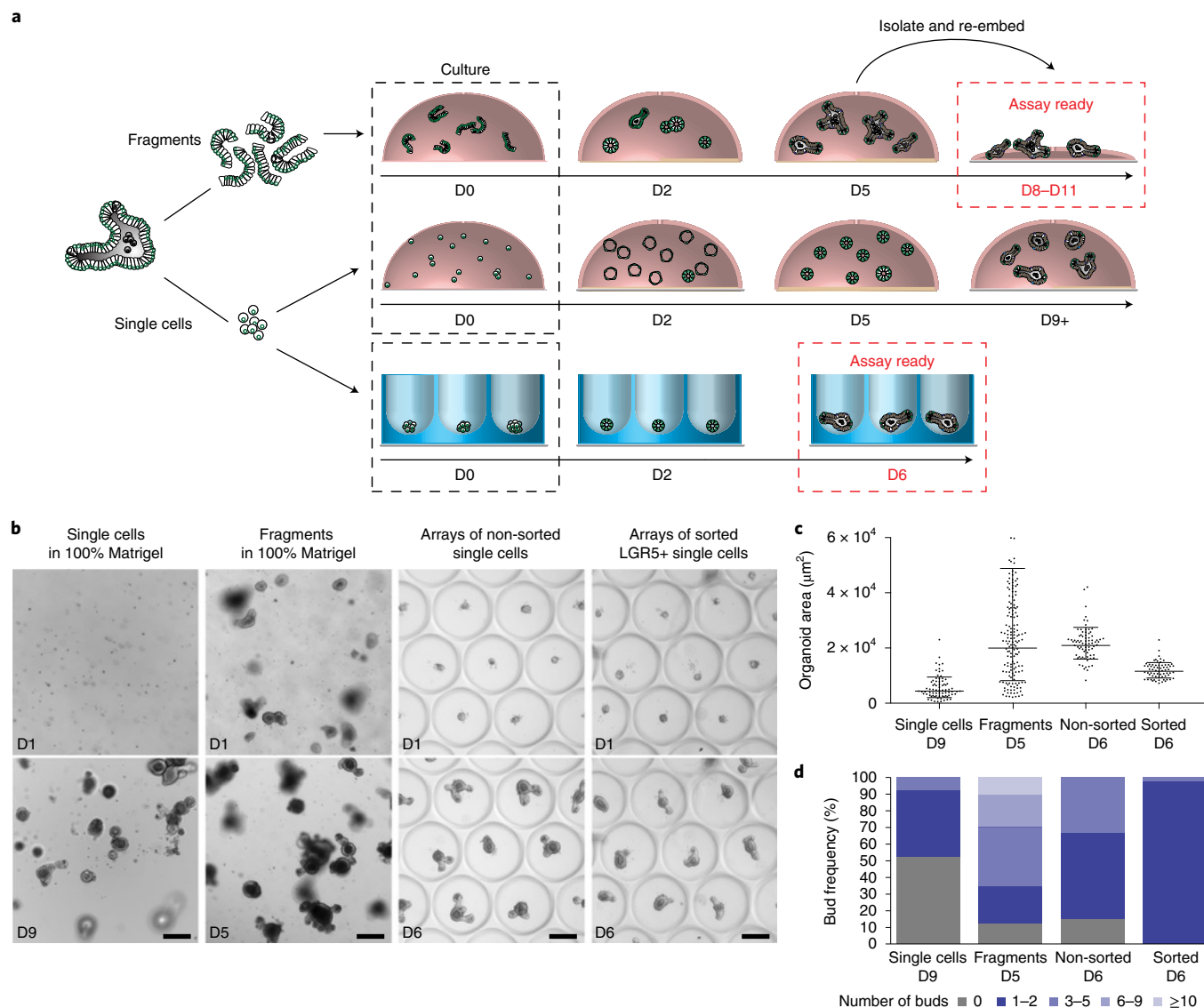


**Fig. 4 | Analysis of organoid homogeneity and reproducibility.** **a**, Schematic of the processing steps in our approach compared with other methods that are available at present. Intestinal organoids grown from fragments mature within 5–6 d but are extremely variable. Organoids grown from single cells display less variability but mature for longer periods. Our method enables the generation of highly reproducible assay-ready organoids in very short periods. Matrigel consumption using our system is decreased 20- to 50-fold compared with other methods. **b**, Representative wide-field images of cultures on the first day and at the end point started from single cells or fragments in Matrigel drops and from arrays containing 100 single cells, FACS-sorted or non-sorted, per microwell. Scale bars, 200  $\mu\text{m}$ . **c,d**, Organoid area distributions (**c**) from one representative experiment and bud frequency analysis (**d**) at the end point of the culture pooled from two independent experiments.

collagen IV would reflect their respective concentration in 2% Matrigel. We observed that organoids can be grown in microcavity arrays when exposed to laminin-111 (Supplementary Fig. 3a) alone, whereas culture in collagen IV alone resulted in poor cell survival (Supplementary Fig. 3b). Notably, our approach is also amenable to the efficient culture of human epithelial organoids such as those from the colon (Supplementary Fig. 4a–c) and from induced-pluripotent-SC- (iPSC)-derived intestinal stem/progenitor cells (Supplementary Fig. 4d–f).

One of the major limitations of conventional organoid cultures performed in 3D matrices such as Matrigel<sup>3</sup> or chemically defined hydrogels<sup>19</sup> is the lack of accessibility for downstream analyses, as they are embedded in a solid matrix. Enzymatic digestion or mechanical dissociation can be used to release organoids from these

cultures but at the expense of traceability. The open, solid-matrix-free configuration of our cultures offers the unique possibility to pick single organoids of interest for performing downstream analyses, or to further propagate organoids with specific characteristics. As a proof-of-principle, we picked a single intestinal organoid from an array and re-embedded it into a conventional Matrigel culture in which it was readily propagated (Supplementary Fig. 5a–c).

**Improving organoid homogeneity.** The homogeneity and reproducibility of cell cultures is a critical requirement for developing cell-based assays in pharmaceutical drug development and diagnostics. In a next set of experiments, we therefore aimed to systematically assess potential differences in variability among classical Matrigel-based cultures and our microengineered organoid

arrays. Specifically, we compared intestinal organoids grown from (1) single cells in Matrigel, (2) intact crypt fragments in Matrigel, (3) non-sorted (that is, comprising a mixture of ISCs and Paneth cells<sup>11</sup>) single-cell aggregates cultured on microcavity arrays and (4) GFP-sorted (that is, comprising pure ISCs) single-cell aggregates cultured on microcavity arrays (Fig. 4a). We chose organoid area and the number of budding structures within single organoids<sup>20–22</sup> as read-outs at the end point of each culture, which can vary from 5 d to 9 d. This experiment revealed a pronounced difference in heterogeneity between the two approaches, with organoid arrays resulting in far more homogeneous tissues in general (Fig. 4b). We attribute this difference not only to the more controlled starting cell numbers at the onset of the cultures, but also to the potential fusion of organoids that grow in close proximity in Matrigel (Supplementary Fig. 6a–d)—an event that never occurs in spatially controlled microcavity cultures. The size variability of organoids formed from tissue fragments was particularly high, spanning more than two orders of magnitude. By contrast, the distribution of organoids grown from single cells in Matrigel and from aggregates composed of non-sorted cells in microcavity arrays was relatively similar (Fig. 4c). We also found that aggregates of pure Lgr5<sup>+</sup> SCs gave rise to organoid populations with exquisite homogeneity. This suggests that the presence of differentiated cells (for example Paneth cells, which are known to be important mediators of symmetry breaking in intestinal organoids<sup>23</sup>) within organoids grown in SC enrichment medium<sup>16</sup> may contribute to an increased variability, even when starting from homogeneous cell aggregates. Quantification of the frequency of bud formation under the four culture conditions qualitatively mirrored the results of the size distribution (Fig. 4d). Interestingly, the number of tissues without any buds was found to be much higher (>50%) in Matrigel-based single-cell cultures compared with organoid arrays that were generated from non-sorted cells (~10%) or sorted ISCs (0%). Unsurprisingly, organoids that were derived from fragments showed the highest variability in bud numbers, presumably due to the lack of control of the starting cell numbers and the cell types contributing to the final structures, and also due to possible fusion events (Supplementary Fig. 6a–d). Collectively, these data show that aggregated ISCs are an excellent starting point for the highly efficient and rapid generation of organoids in this facile, 3D culture in a 2D plane setting. This strategy enables us to essentially bypass the SC expansion phase that is needed to generate sufficient cells for intestinal organoid formation from single SCs, resulting in a substantial gain in speed. Cell aggregation also contributes to an increased homogeneity and reproducibility by synchronizing growth within a heterogeneous population of individual cells. Moreover, by keeping single organoids in spatially preallocated microcavities, we demonstrate the possibility to trace every individual organoid of an entire population, enabling a correlation of dynamic, morphogenetic behaviours with an end-point assessment of cell fate using downstream assays such as immunocytochemistry and DNA or RNA analyses. Indeed, a detailed comparison of our approach with existing GI organoid-based assays<sup>24,25</sup> revealed

substantial improvements not only in assay speed, but also in medium consumption and costs (Supplementary Table 1).

**High-content phenotypic drug screening.** We next sought to demonstrate the potential of our approach for automated organoid derivation and high-content phenotypic drug testing (Fig. 5). Interfacing hydrogel-based microcavity arrays with standard multiwell cell culture plates enabled us to robotically execute all of the steps of the fabrication of intestinal organoid arrays, including hydrogel substrate preparation, ISC seeding, addition and exchange of culture medium, ISC expansion and organoid formation (Fig. 5a). Importantly, we did not measure any difference in SC colony-formation efficiency between the manual and automated process (Fig. 5b).

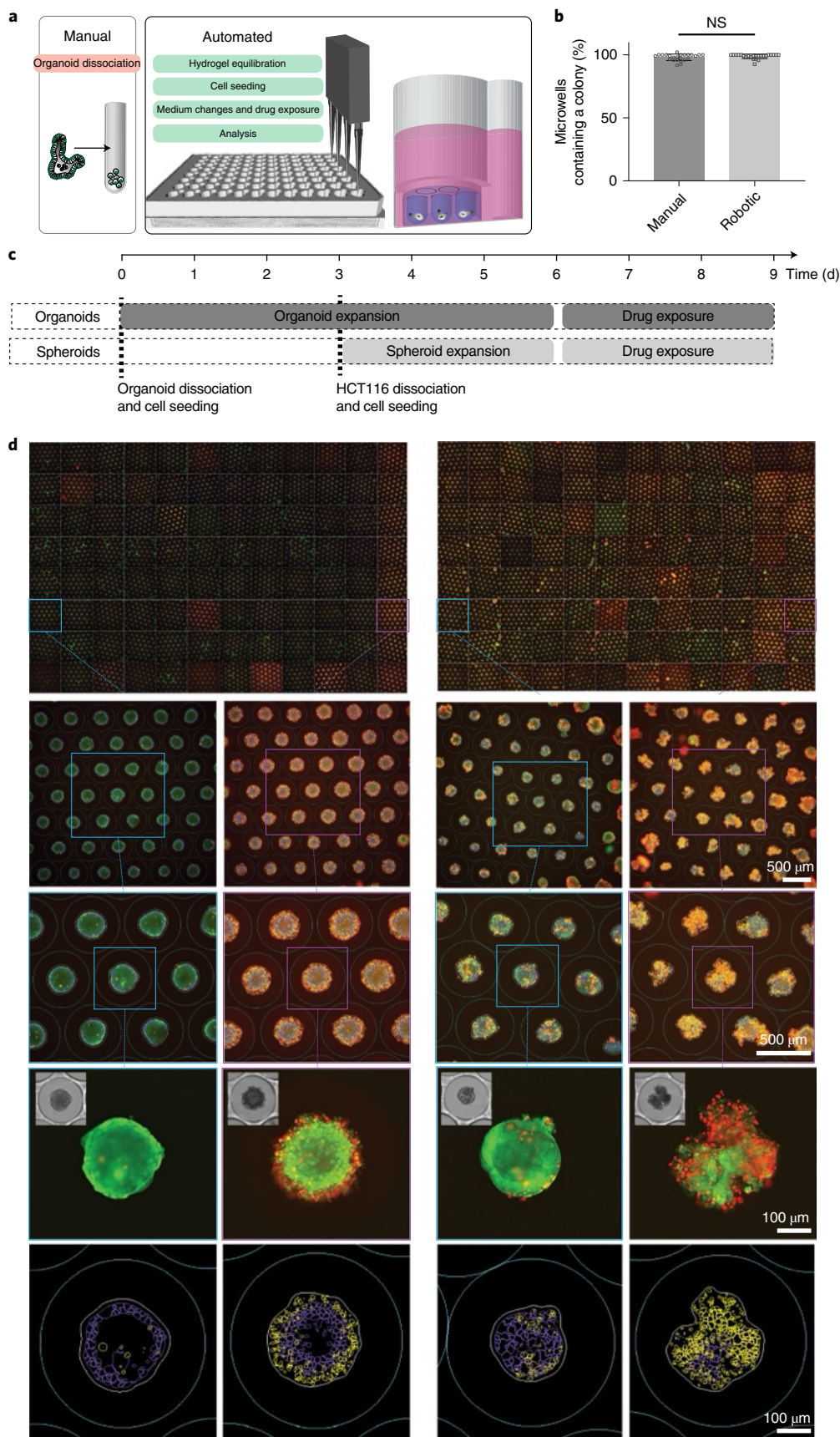
To perform a proof-of-concept high-content phenotypic drug screen, we focused on human CRC tumoroids derived from a primary colorectal tumour resection and tested 80 compounds that are either FDA-approved or in clinical trials (Fig. 5c, Supplementary Fig. 7a–g). As a benchmark, we used arrays of spheroids generated from human colon carcinoma cells (HCT116 cell line) produced on our hydrogel-based microcavity arrays. After 3 d of drug exposure, microtissue viability was tested and phenotypically analysed using high-throughput imaging and automated high-content analyses. We extracted more than 250 features from each microtissue (Fig. 5d, Supplementary Fig. 8a–f) and computed their multivariate linear discriminant (LDA) projections to determine the most effective compounds. LDA projections of the positive (gambogic acid; Supplementary Video 3) and the negative (DMSO; Supplementary Video 4) controls validated the Z-factor  $Z'$  of the screening assay and enabled us to linearly classify efficiencies of the screened compounds (Figs. 5d and Fig. 6a) from up to 40 microtissues per field of view (Fig. 6b) without the need to exclude false-positives<sup>12</sup>. Importantly, our screening is highly reproducible for both CRC tumoroids and HCT116 spheroids with Pearson's coefficients of 0.9 and 0.79, respectively (Fig. 6c,d), revealing that tumoroids are highly sensitive to chemotherapy and epidermal growth factor receptor (EGFR) inhibitors compared with HCT116 spheroids (Fig. 6e). As the donor patient received surgery in the adjuvant setting, in which genomic analysis of the tumour is not warranted, no clinical analysis of the mutation status of *KRAS* was performed. However, to define the *KRAS* mutation status of the organoids, we analysed RNA sequencing (RNA-seq) data using the GenomeAnalysisToolkit (GATK v.4) pipeline. We could not detect mutations in exome 2 and exome 3 of *KRAS* (Supplementary Fig. 9), explaining the responsiveness to EGFR inhibitors, especially in the presence of the EGF ligand. By contrast, HCT116 cells have a *KRAS* mutation and are therefore non-responsive to EGFR inhibition, in line with the results from the screen.

Principal component analysis (PCA) on multivariate imaging dataset (Supplementary Fig. 10) uncovered three strong phenotypic outliers, namely orantinib, vindesine and afuresertib (Fig. 7a). Interestingly, the AKT inhibitor afuresertib induced major swelling of the cystic tumoroids between 48 h and 72 h (at 1  $\mu$ M;

**Fig. 5 | Automated high-content phenotypic drug screening.** **a**, Schematic of an automated fabrication of mouse intestinal organoid arrays. Organoids in expansion conditions (from Matrigel drops in self-renewal medium) were dissociated manually. The resulting solution was placed into the robotic liquid handling system. The automatic liquid-handling system was able to deposit mouse ISCs and handle the appropriate growth medium reliably without any human interference. **b**, The percentage of microwells containing a SC colony after 2–3 d of culture. No differences were observed between a manually or a robotically generated organoid array. Data are mean  $\pm$  s.d.;  $n = 24$ , pooled from two independent robotic dispensing experiments, Manual,  $98.1 \pm 2.6\%$  (centre value  $\pm$  s.d.); robotic,  $98.8 \pm 1.8\%$ . NS, not significant. **c**, The timeline of the screening protocol. **d**, Tiled fluorescence microscopy images of one 96-well plate replicate of the screen. The microtissues were fluorescently labelled with calcein-AM (live, green) and ethidium homodimer-1 (dead, red). The left column shows HCT116 microtissues and the right column shows CRC organoids. As representative examples, the positive and the negative controls were chosen to demonstrate our automated imaging pipeline. The bottom row shows the corresponding outlines of objects segmented during image analysis for the above microscopy images; microcavities are shown in cyan, spheroids or organoids are shown in white, live cells are shown in purple and dead cells are shown in yellow. Scale bars, 500  $\mu$ m (second and third row) and 100  $\mu$ m (fourth and fifth row).

Supplementary Video 5)—a phenotype that was not observed in compact HCT116 spheroids (Fig. 7b). A dose-response analysis showed that afuresertib displays apparent toxicity at 20  $\mu$ M (Fig. 7c),

whereas the swelling phenotype was observable only at intermediate concentrations and in a defined window between 0.3  $\mu$ M and 4  $\mu$ M (Fig. 7d, Supplementary Fig. 11), with a half-maximum



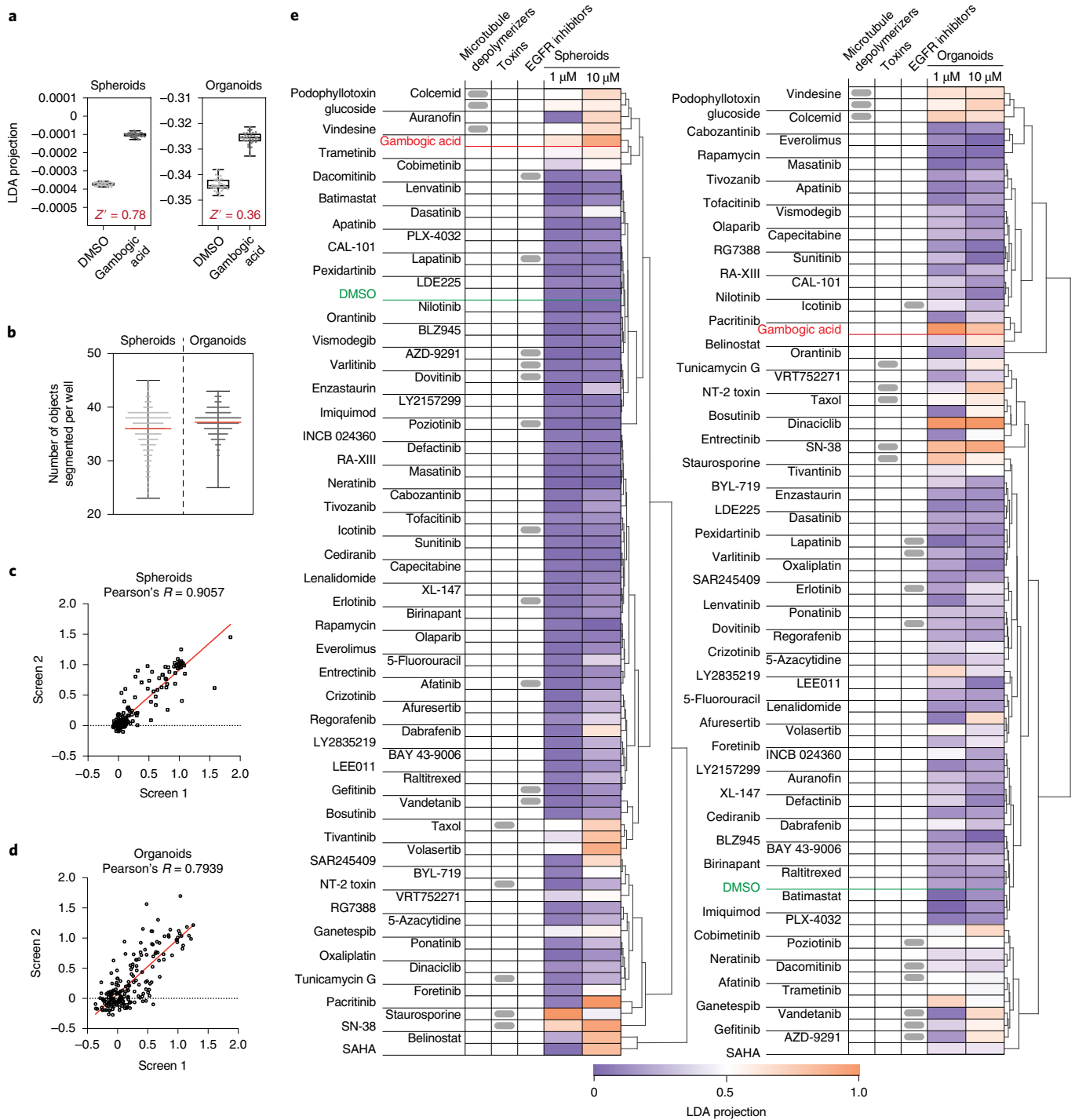


**Fig. 6 | Organoid phenotypic drug screening performances and hit map.** **a**, Comparison of the LDA projection average values and their variability between both the positive and negative controls as well as between HCT116 spheroids and CRC organoids. **b**, The average number of microtissues detected per field of view using the automated image-analysis pipeline. **c,d**, Correlation of the results between the different screen replicates for HCT116 spheroids (**c**) and CRC organoids (**d**). **e**, Heat map of the LDA projection scores of our 80 chosen compounds after hierarchical clustering according to all of the extracted features. Specific families of compounds are noted, such as microtubule depolymerizers, toxins and EGFR inhibitors. The positive gambogic acid and the negative DMSO controls are indicated in red and green, respectively.

inhibitory concentration ( $IC_{50}$ ) value at  $0.31 \mu\text{M}$  (Fig. 7e). Thus, an image-based analysis of individual organoids revealed phenotypes that are not observable using conventional screening approaches based on a bulk read-out (toxicity), occurring only at high concentrations, with a specific  $IC_{50}$  of  $10.67 \mu\text{M}$  (Fig. 7f,g).

To investigate the potential mechanisms by which afuresertib exerts its swelling effect, we performed RNA-seq analysis of tumouroids, in the presence and absence of afuresertib, grown in microengineered substrates as well as conventional 3D Matrigel (Supplementary Fig. 12a). Gene Ontology (GO) term analysis revealed that the

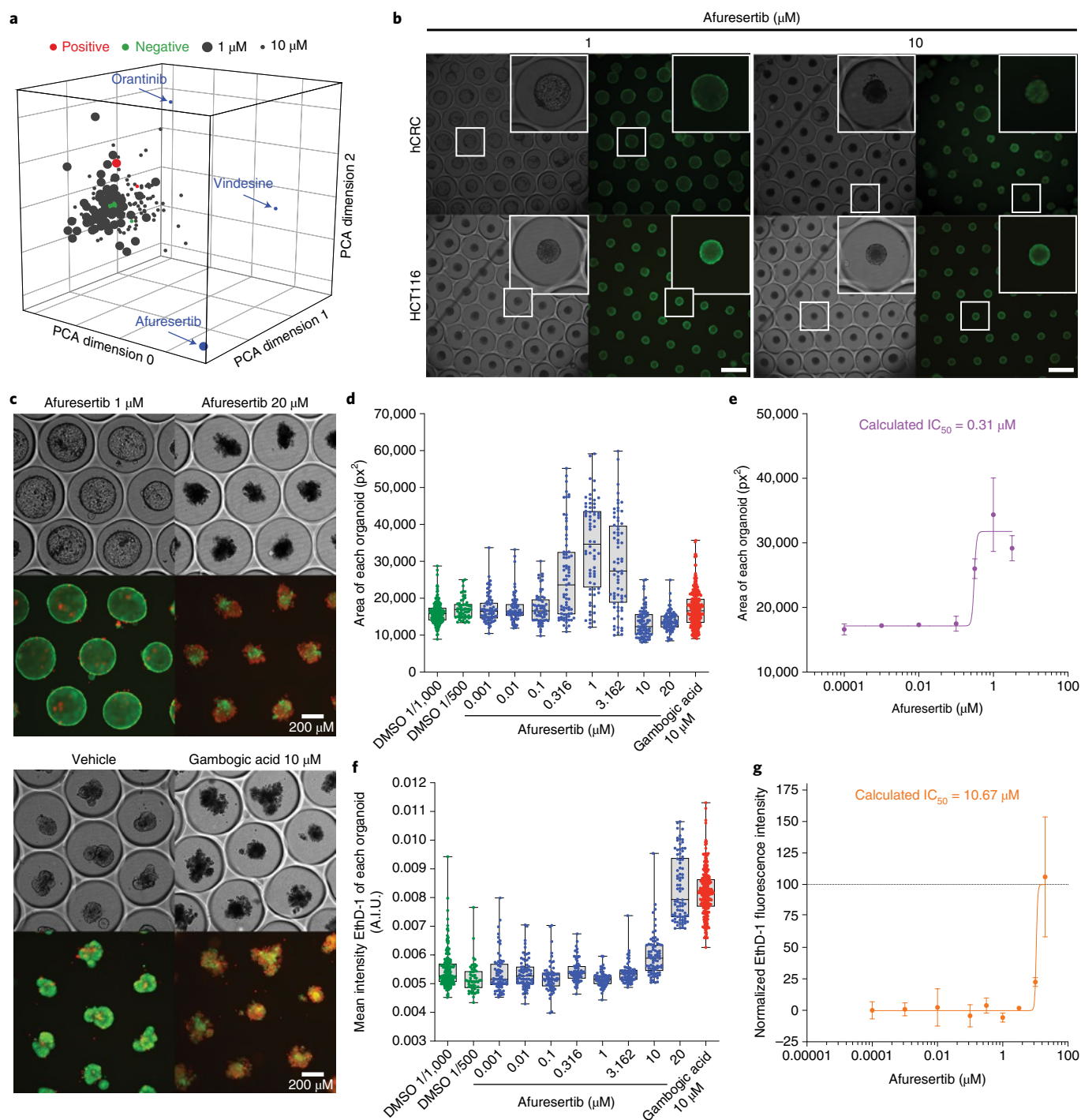


**Fig. 7 | Phenotypic hit analysis.** **a**, Three-dimensional representation of the PCA values of the 72 compounds at 1  $\mu\text{M}$  (large dots) and 10  $\mu\text{M}$  (small dots) along the dimensions 0, 1 and 2, representing microtissue morphology, live cells and dead cells, respectively. The positive (gambogic acid) and the negative (DMSO) controls are highlighted in red and green. The arrows indicate the outliers, afuresertib, orantinib and vindesine. **b**, Comparative wide-field and fluorescence microscopy images showing the effect of afuresertib at 1  $\mu\text{M}$  and 10  $\mu\text{M}$  on CRC organoids and HCT116 spheroids. Scale bars, 200  $\mu\text{m}$ . **c**, Representative wide-field and fluorescence microscopy images of the effect of afuresertib on CRC organoids at various concentrations in comparison with the positive (gambogic acid) and negative (DMSO) controls. For **b** and **c**, the microtissues were fluorescently labelled with calcein-AM (live, green) and ethidium homodimer-1 (dead, red). Scale bar, 200  $\mu\text{m}$ . **d**, **e**, The phenotypic response of CRC organoids exposed to increasing concentrations of afuresertib, characterized by microtissues area (**d**) was measured and the specific phenotypic  $\text{IC}_{50}$  value (**e**) was found to be 0.31  $\mu\text{M}$ . For **d** and **e**, data are shown in  $\text{px}^2$ , where 1 px corresponds to 1.625  $\mu\text{m}$ . **f**, **g**, The measured viability of CRC organoids (**f**; mean intensity of ethidium homodimer-1 staining for each organoid) when exposed to increasing concentrations of afuresertib, and its associated  $\text{IC}_{50}$  value (**g**), calculated at 10.67  $\mu\text{M}$ . For **g**, data were normalized to the corresponding controls (DMSO and gambogic acid) set as 0 and 100. Data are mean  $\pm$  s.d., pooled from two independent screens.

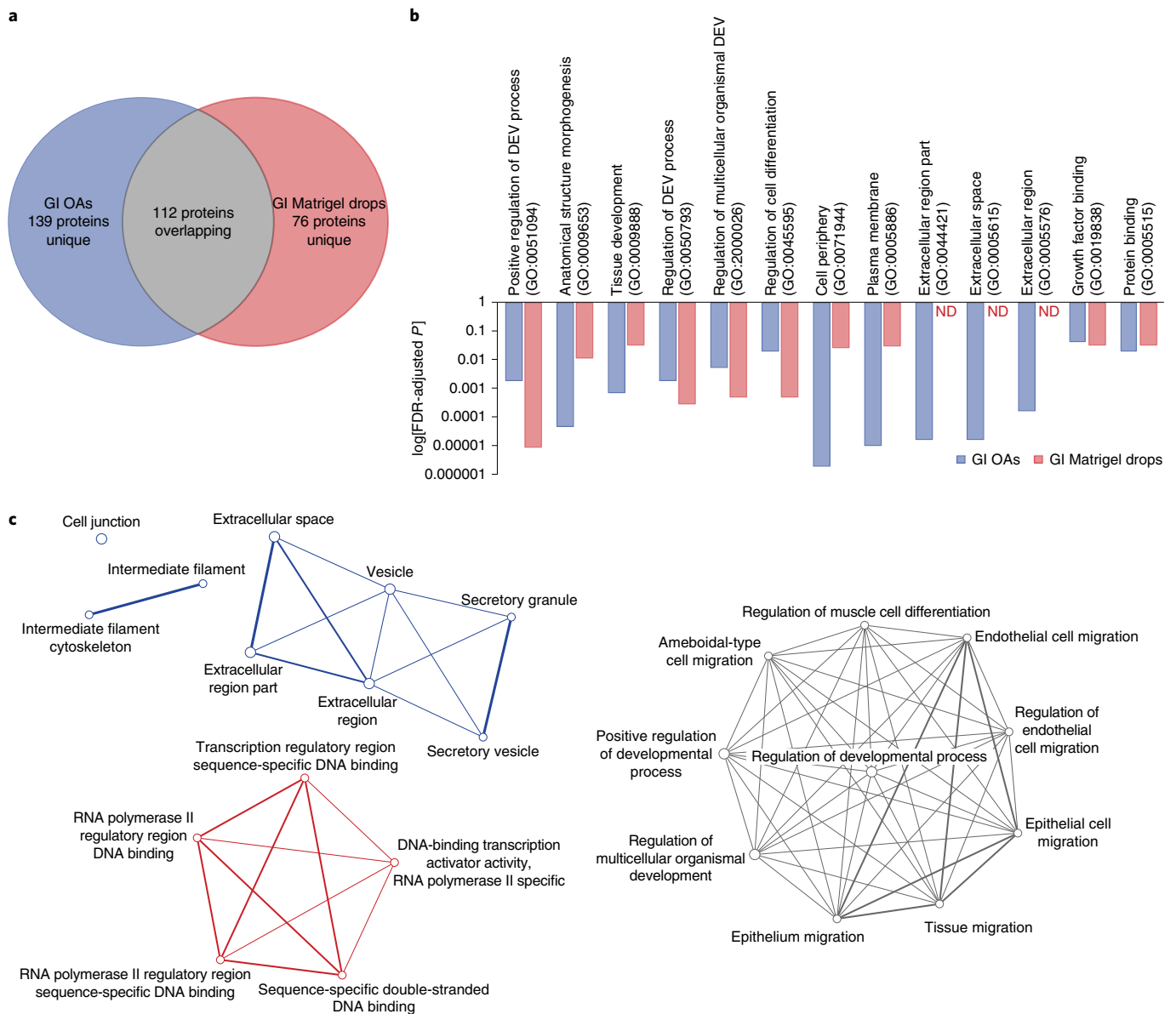


**Fig. 8 | RNA-seq analysis. a–c,** Proportion of genes (**a**), most significant GO terms (**b**) and network analysis (**c**) extracted from the genes showing an increase of expression of 1.5-fold ( $\log_2$ -transformed fold change) in  $1\mu\text{M}$  afuresertib compared with vehicle. GI organoid arrays (OAs) are indicated in blue and GI Matrigel drops are indicated in red. DEV, developmental; GO, gene ontology; ND, not detected.

morphological change is linked to the overexpression of about 100 genes that are involved in morphogenesis, development and differentiation (Fig. 8a). Notably, afuresertib seems to exert its action not by altering fluid transport through the epithelium, but rather by inducing potentially EMT-related processes such as cell migration (Fig. 8a,c, grey; Supplementary Fig. 12b). Overall, we found that 112 upregulated genes are shared among the two culture conditions. We found that 139 genes, which are significantly involved in the production of ECM components and the surrounding microenvironment (Fig. 8a,c, blue; Supplementary Fig. 12b), were exclusively upregulated in tumouroids derived on the microengineered hydrogel substrates; and 76 genes, which are primarily involved in DNA binding and processing (Fig. 8a,c, red; Supplementary Fig. 12b), were upregulated in Matrigel drops only (Fig. 8b, Supplementary Fig. 12b). A major difference in the derivation of organoids in microengineered arrays versus 3D Matrigel is that the former is performed in the presence of low concentrations (2%) of soluble Matrigel, which we hypothesize may trigger enhanced secretion of the cells own ECM. It would be an interesting

endeavour for future studies to explore what type of ECM is deposited by the tissues in the two culture conditions, and whether a potential difference could result in disparate organoid cell type composition and behaviour.

## Discussion

We present a robust and versatile approach to standardize and automate the fabrication and analysis of mouse and human GI organoids. Previous attempts to fabricate organoid arrays have either focused on growing intestinal organoid fragments on a Matrigel bed or on polystyrene-coated PDMS substrates<sup>9–13</sup>. Although these strategies have improved the multiplexing and imaging abilities of organoids, they do not readily provide the possibility to fully automate organoid culture for high-throughput and high-content organoid-based screening. Thus, our approach offers several key advantages compared with existing microwell-based technologies or 3D organoid culture systems. These include the versatility of customizing the physical and chemical properties of the hydrogel

substrates, a reduction in heterogeneity of the final tissues, as well as an increase in growth speed, single-organoid traceability from initial cell seeding to downstream analysis and accessibility. Furthermore, our culture system leads to a considerable reduction in expensive reagent consumption, which is particularly relevant for large-scale screening approaches. We therefore believe that our technology provides avenues for robotized high-content screening of tissue-level function based on organoid cultures.

## Methods

**Fabrication of hydrogel-based U-bottom microwell arrays.** U-shaped microcavities of any size between 10  $\mu\text{m}$  and 1.5 mm were generated onto standard four-inch silicon wafers using standard Si Bosch in combination with soft lithography processes<sup>14</sup>. PDMS (ratio 1:10, cross-linking agent:elastomer (SYLGARD 184 Silicone Elastomer Kit, Dow Corning)) was then poured onto the wafers and cured overnight at 75 °C. After cross-linking, the PDMS stamps were demoulded and punched with various diameters. The desired stamps were mounted on custom-made epoxy holders (SIKA Sikadur-52 Injection). As shown in Supplementary Fig. 1a, the final non-cross-linked hydrogel mix was deposited onto the PDMS stamp, and the holder-stamp-hydrogel construct was placed into a custom-made PDMS ring that was preplaced at the bottom of the wells of a 24-well plate. The hydrogels were incubated at 37 °C and 5% CO<sub>2</sub> for 15 min to 1 h depending on the type of hydrogel used (see below). After cross-linking, aqueous buffer (for example, 1× PBS) was pipetted into the wells and the holders-stamps were removed carefully. The resulting microwell arrays were sterilized thoroughly in buffer under ultraviolet light and stored at 4 °C after use. Arrays (width, 6 mm) containing microcavities of 500  $\mu\text{m}$  in diameter, 600  $\mu\text{m}$  in height and equally spaced (40  $\mu\text{m}$ ) were used to generate intestinal organoid arrays.

**Preparation of hydrogels.** PEG hydrogels, which were cross-linked by Michael-type addition reaction, were prepared as described previously<sup>15</sup>, mixing aqueous solutions containing thiol- and vinylsulfone-functionalized 4arm-PEG and 8arm-PEG macromers (molecular mass, 10 kDa and 40 kDa, respectively) at various concentrations to adjust stiffness and stoichiometric ratio. The solution was deposited and moulded as explained above. The construct was cross-linked for 15 min at room temperature. Gelatin (porcine high strength, Fluka) was solubilized at 10% w/v. The solution was deposited and moulded as described above. The construct was cross-linked for 2 h at 37 °C and 5% CO<sub>2</sub>. Agarose (standard molecular biology grade, Eurobio, Brunshwig) was solubilized at 2% w/v and heated to reach full solubility. The solution was deposited and moulded as described above. The construct was cross-linked for 1 h at 4 °C. Alginate (PRONOVA, low viscosity sodium alginate, FMC biopolymer/Novamatrix) was solubilized at 2% w/v. The solution was deposited and moulded as described above. The construct was exposed to a solution of calcium chloride (CaCl<sub>2</sub>) at 100 mM for 4 h at room temperature to ensure homogenous cross-linking.

**Cell culture.** Mouse crypts were extracted from the small intestines of LGR5-eGFP reporter mice as described previously<sup>19</sup>. The isolated crypts were maintained and expanded in Matrigel in ISC expansion medium (ENR-CV; Advanced DMEM/F12 containing Glutamax, HEPES, penicillin-streptomycin, B-27 (Life technologies), 1mM *N*-acetylcysteine (Sigma-Aldrich) supplemented with the growth factors EGF (50 ng ml<sup>-1</sup>; R&D), noggin (100 ng ml<sup>-1</sup>; produced in-house) and R-spondin (500 ng ml<sup>-1</sup>; produced in-house), and the small molecules CHIR99021 (3  $\mu\text{M}$ ; Millipore) and valproic acid (1 mM; Sigma-Aldrich)<sup>16,19</sup>. The organoids were maintained and expanded as follows: growth factors were replenished every second day, the full medium was changed every 4 d and the cells were passaged every 3–4 d.

Human colon organoids were generated as reported previously<sup>6</sup>. The isolated crypts were grown in drops of Matrigel gel (20  $\mu\text{l}$ ) overlaid with hCSC expansion medium comprising Advanced DMEM/F12 containing Glutamax, HEPES, penicillin-streptomycin, B27 (Life technologies), 1mM *N*-acetylcysteine (Sigma-Aldrich), Wnt3A (conditioned medium produced in house, 50%), EGF (50 ng ml<sup>-1</sup>; R&D), noggin (100 ng ml<sup>-1</sup>; produced in-house), R-spondin (500 ng ml<sup>-1</sup>; produced in-house), nicotinamide (10  $\mu\text{M}$ , Sigma-Aldrich), gastrin (10 nM, Sigma-Aldrich), A83-01 (500 nM, Tocris), SB202190 (10  $\mu\text{M}$ , Sigma-Aldrich), prostaglandin-E2 (10 nM; Tocris) and Y-27632 (10  $\mu\text{M}$ , Abmole). The full medium was replaced every 2–3 d and the cells were passaged every 7–10 d.

Human iPSC-derived intestinal organoids were generated as described previously<sup>26</sup>. Organoids were maintained and expanded as follows: the full expansion medium (Advanced DMEM/F12 containing Glutamax, HEPES, penicillin-streptomycin, N-2 (Life technologies), B-27 (Life technologies), *N*-acetylcysteine (1 mM; Sigma-Aldrich), EGF (50 ng ml<sup>-1</sup>; R&D), noggin (100 ng ml<sup>-1</sup>; produced in-house), R-spondin (500 ng ml<sup>-1</sup>; produced in-house), nicotinamide (10 mM, Sigma-Aldrich), A83-01 (500 nM, Tocris), prostaglandin-E2 (2.5  $\mu\text{M}$ ; Tocris), Wnt3A (100 ng ml<sup>-1</sup>; R&D) and Y-27632 (10  $\mu\text{M}$ , Abmole) was changed every 2–3 d and the cells were passaged every 7–10 d.

HCT116 (human colorectal carcinoma) cell line was purchased from ATCC and was used between passage numbers 10 and 35. Cells were grown and maintained as adherent monolayer cultures in 75 cm<sup>2</sup> culture flasks (TPP) without antibiotics using

McCoy5a Medium (McCoy5a, GlutaMAX, 36600–021, Gibco Life Technologies), supplemented with 10% heat-inactivated fetal bovine serum (FBS, Invitrogen 10101–145) at 37 °C in a humidified CO<sub>2</sub> incubator. Cells were subcultured 2–3 times per week using Trypsin-EDTA (0.05%; Life Technologies, 25300062) and diluted with growth medium (1:5 to 1:20). For the assay, cells were collected from culture at confluence between 60% and 80%, while cell viability was >90%.

Human colorectal tissues were obtained from the Centre Hospitalier Universitaire Vaudois with informed consent. The study was approved by the local regulatory body, CER-VD, under the ID 2017-00359. The primary tumour resections were processed as described previously<sup>12,27</sup>, and the organoids were expanded and maintained in advanced DMEM/F12 containing Glutamax, HEPES, penicillin-streptomycin, B-27 (Life technologies), 1mM *N*-acetylcysteine (Sigma-Aldrich) supplemented with the growth factors EGF (50 ng ml<sup>-1</sup>; R&D) and noggin (100 ng ml<sup>-1</sup>; produced in-house). The organoids were maintained and expanded as follows: the full medium was changed every 3 d and the cells were passaged every 6–8 d.

## Preparation of mouse intestinal organoids and human healthy or CRC organoid arrays.

LGR5-GFP intestinal organoids or human organoids were released from Matrigel in cold basal medium (advanced DMEM/F-12 containing 1 mM HEPES, Glutamax and 1% penicillin-streptomycin). The organoids were centrifuged at 800 r.p.m. for 4 min at 4 °C and resuspended in 1 ml of cell dissociation solution (TrypLE, 2 mg ml<sup>-1</sup> DNase I (Gibco), 1mM *N*-acetylcysteine and 10  $\mu\text{M}$  Y27632, or just TrypLE in the case of human colon organoids). Cells were dissociated for 8 min at 37 °C and were subsequently washed with basal medium containing 10% heat-inactivated FBS (Gibco). After centrifugation at 1,000 r.p.m. for 4 min at 4 °C, the cells were resuspended at the appropriate density in ENR-CV medium or human colon, iPSC-derived SC or CRC organoids expansion medium supplemented with 2.5  $\mu\text{M}$  thiazovivin or 10  $\mu\text{M}$  Y27632 to deposit typically 100 cells per microwell. The final cell suspension (50  $\mu\text{l}$ ) was added onto each microwell array. The cells were allowed to sediment for 30 min as such and 150  $\mu\text{l}$  of self-renewal medium, supplemented with 2% Matrigel (Corning, 356231, 9021357), 142.8  $\mu\text{g}$  ml<sup>-1</sup> Cultrex 3D laminin I or 79.1  $\mu\text{g}$  ml<sup>-1</sup> collagen type IV when applicable (ENR-CV or human colon SC or iPSC-derived stem/progenitor cells expansion medium), was added to each well. For mouse organoid arrays and human iPSC-derived organoid arrays, the resulting colonies were expanded in self-renewal medium for 3 d, and the organoids were differentiated for another 3 d in differentiation medium (ENR for mouse, and SC expansion medium without nicotinamide and Wnt3A for human iPSC-derived organoids, respectively)<sup>16</sup>. Growth factors were replenished every other day and the full medium was replaced every 4 d. For human colon, CRC organoid and HCT116 spheroid arrays, 200 cells were seeded per microwell, the colonies were kept in expansion medium and the full medium was replaced every 2–3 d. For HCT116 cells, no Matrigel was added to the medium.

**On-array immunohistochemistry.** Mouse intestinal organoid arrays were washed carefully three times with 1× PBS and fixed with 4% PFA for 30 min at room temperature without shaking. The samples were then washed thoroughly three times with 1× PBS and permeabilized with 0.2% Triton X-100 in 1× PBS for 30 min at room temperature. The samples were then blocked with 10% goat serum in 1× PBS containing 0.02% Triton X-100 for 4 h at 4 °C. Primary antibodies against L-FABP (host, rabbit; dilution, 1:50; Santa Cruz, sc-50380), lysozyme (host, rabbit; dilution, 1:50; Thermo Fisher Scientific, PA1-29680), chromogranin-A (host, rabbit; dilution, 1:50; Santa Cruz, sc-13090), mucin-2 (host, rabbit; dilution, 1:50; Santa Cruz, sc-15334) and SOX-9 (host, rabbit; dilution, 1:50; ab185966) were then added in the blocking buffer and incubated overnight at 4 °C. The primary antibodies were then washed thoroughly and secondary antibodies against Alexa-647 goat-anti-rabbit (dilution, 1:1,000; Invitrogen), Phalloidin (dilution, 1:200, Life Technologies) and DAPI (dilution, 1:1,000, Sigma-Aldrich) in blocking solution were added and incubated overnight at 4 °C. Finally, the samples were washed thoroughly for at least 4 h and imaged using a Zeiss LSM700 inverted confocal microscope.

**Image analysis and quantification.** Organoid areas and number of buds per organoid were analysed using the open access Fiji (ImageJ) software. To quantify the area, the organoids were segmented by subtracting the scanned image of the microwell arrays containing organoids from a scanned image of a microwell array containing no organoids. The organoids were then segmented and binarized, and their specific area was analysed using Fiji's Analyze Particle plugin and saved on the region of interest manager. The entire procedure was automated. The bud numbers of the detected organoids were quantified manually. All of the plots were generated using Prism 7 software (GraphPad).

**CRC organoid and HCT116 spheroid screening.** Organoid and spheroid arrays were generated as described above. Once the microtissues were grown—that is, 6 d and 3 d of expansion for CRC organoids and HCT116, respectively—they were exposed to all 80 selected compounds for a further 3 d. The resulting microtissues were labelled with calcein-AM and ethidium homodimer-1 according to the manufacturer's protocol (Live/DEAD Viability/Cytotoxicity Kit for mammalian cells, Thermo Fisher Scientific) and were imaged using an IN Cell Analyzer 2200 (GE Healthcare). Automated acquisition was performed in an environmental chamber (at 37 °C with 5% CO<sub>2</sub>) using a  $\times 4/0.2\text{NA}$  objective. The entire screens and the dose-response experiments were repeated twice.

**Automated image analysis pipeline and data-analysis workflow.** All of the images were analysed using CellProfiler v.3.1.8 (<https://cellprofiler.org/citations/>)<sup>28</sup> and extracted data were processed through a workflow in Knime (<https://www.knime.com/>). A scheme of the image analysis and data workflow is provided in Supplementary Fig. 8a–f.

**RNA-seq analysis of CRC organoids.** CRC organoids grown in organoid arrays or Matrigel drops exposed to 1  $\mu$ M afuresertib or vehicle were lysed and the mRNA was extracted using the RNeasy mini kit according to the supplier's information. The different samples were quality-controlled using a TapeStation 4200 (Agilent) and sequenced using an Illumina NextSeq500 system. An average of 41 million reads per sample was uniquely aligned to the hg38 human reference genome (GRCh38) using STAR (v.2.5)<sup>29</sup>, and about 90% of those were confidently assigned to genes (GENCODE primary assembly v.27) using HTSeq-count (v.0.9)<sup>30</sup>. Genes with less than 50 reads in all 4 samples were excluded, and the log<sub>2</sub>-normalized counts per million values of the remaining 13,668 genes were calculated using the R package edgeR (v.3.14)<sup>31</sup>. The GO analysis was performed using the online tool string-db.org and the Venn diagram was generated using the online tool at <http://bioinformatics.psb.ugent.be/webtools/Venn/>. Mutation calling from the four set of the RNA-seq experiment organoids were analysed using the GATKv4 pipeline. Mutations in exome 2 and exome 3 of *KRAS* were analysed using the reference of the Broad Institute, GATK Best Practices 2017, (<https://software.broadinstitute.org/gatk/best-practices/>; accessed 12 August 2017). The pipeline did not find any mutations in the regions of exome 2 and 3.

**Reporting Summary.** Further information on research design is available in the Nature Research Reporting Summary linked to this article.

### Data availability

The main data supporting the results in this study are available within the paper and its Supplementary Information. The raw and analysed datasets generated during the study are too large to be publicly shared, yet they are available for research purposes from the corresponding author on reasonable request. The RNA-seq data have been deposited at the NCBI Gene Expression Omnibus, and are accessible under the GEO Series accession number [GSE148347](https://www.ncbi.nlm.nih.gov/geo/query/acc.cgi?acc=GSE148347).

Received: 24 October 2019; Accepted: 29 April 2020;

Published online: 08 June 2020

### References

- Lancaster, M. A. & Knoblich, J. A. Organogenesis in a dish: modeling development and disease using organoid technologies. *Science* **345**, 1247125 (2014).
- Dutta, D., Heo, I. & Clevers, H. Disease modeling in stem cell-derived 3D organoid systems. *Trends Mol. Med.* **23**, 393–410 (2017).
- Fatehullah, A., Tan, S. H. & Barker, N. Organoids as an in vitro model of human development and disease. *Nat. Cell Biol.* **18**, 246–254 (2016).
- Ranga, A., Gjorevski, N. & Lutolf, M. P. Drug discovery through stem cell-based organoid models. *Adv. Drug Deliv. Rev.* **69–70**, 19–28 (2014).
- Sato, T. et al. Single Lgr5 stem cells build crypt-villus structures in vitro without a mesenchymal niche. *Nature* **459**, 262–265 (2009).
- Sato, T. et al. Long-term expansion of epithelial organoids from human colon, adenoma, adenocarcinoma, and Barrett's epithelium. *Gastroenterology* **141**, 1762–1772 (2011).
- Akkerman, N. & Defize, L. H. K. Dawn of the organoid era: 3D tissue and organ cultures revolutionize the study of development, disease, and regeneration. *Bioessays* <https://doi.org/10.1002/bies.201600244> (2017).
- Schneeberger, K. et al. Converging biofabrication and organoid technologies: the next frontier in hepatic and intestinal tissue engineering? *Biofabrication* **9**, 013001 (2017).
- Gracz, A. D. et al. A high-throughput platform for stem cell niche co-cultures and downstream gene expression analysis. *Nat. Cell Biol.* **17**, 340–349 (2015).
- Gunasekara, D. B. et al. Development of arrayed colonic organoids for screening of secretagogues associated with enterotoxins. *Anal. Chem.* **90**, 1941–1950 (2018).
- Francies, H. E., Barthorpe, A., McLaren-Douglas, A., Barendt, W. J. & Garnett, M. J. Drug sensitivity assays of human cancer organoid cultures. *Methods Mol. Biol.* **1576**, 339–351 (2019).
- van de Wetering, M. et al. Prospective derivation of a living organoid biobank of colorectal cancer patients. *Cell* **161**, 933–945 (2015).
- Vlachogiannis, G. et al. Patient-derived organoids model treatment response of metastatic gastrointestinal cancers. *Science* **359**, 920–926 (2018).
- Wang, Y. et al. A microengineered collagen scaffold for generating a polarized crypt-villus architecture of human small intestinal epithelium. *Biomaterials* **128**, 44–55 (2017).
- Gobaa, S. et al. Artificial niche microarrays for probing single stem cell fate in high throughput. *Nat. Methods* **8**, 949–955 (2011).
- Yin, X. et al. Niche-independent high-purity cultures of Lgr5<sup>+</sup> intestinal stem cells and their progeny. *Nat. Methods* **11**, 106–112 (2014).
- Sato, T. et al. Paneth cells constitute the niche for Lgr5 stem cells in intestinal crypts. *Nature* **469**, 415–418 (2011).
- Zhang, Y., Lukacova, V., Reindl, K. & Balaz, S. Quantitative characterization of binding of small molecules to extracellular matrix. *J. Biochem. Biophys. Methods* **67**, 107–122 (2006).
- Gjorevski, N. et al. Designer matrices for intestinal stem cell and organoid culture. *Nature* **539**, 560–564 (2016).
- Pastula, A. et al. Three-dimensional gastrointestinal organoid culture in combination with nerves or fibroblasts: a method to characterize the gastrointestinal stem cell niche. *Stem Cells Int.* **2016**, 3710836 (2016).
- Horvay, K. et al. Snai1 regulates cell lineage allocation and stem cell maintenance in the mouse intestinal epithelium. *EMBO J.* **34**, 1319–1335 (2015).
- Yang, T.-L. B. et al. Mutual reinforcement between telomere capping and canonical Wnt signalling in the intestinal stem cell niche. *Nat. Commun.* **8**, 14766 (2017).
- Sato, T. & Clevers, H. Growing self-organizing mini-guts from a single intestinal stem cell: mechanism and applications. *Science* **340**, 1190–1194 (2013).
- Dekkers, J. F. et al. A functional CFTR assay using primary cystic fibrosis intestinal organoids. *Nat. Med.* **19**, 939–945 (2013).
- Ley, S. et al. Screening of intestinal crypt organoids: a simple readout for complex biology. *SLAS Discov.* **22**, 571–582 (2017).
- Hannan, N. R. F. et al. Generation of multipotent foregut stem cells from human pluripotent stem cells. *Stem Cell Rep.* **1**, 293–306 (2013).
- Fujii, M. et al. A colorectal tumor organoid library demonstrates progressive loss of niche factor requirements during tumorigenesis. *Cell Stem Cell* **18**, 827–838 (2016).
- Carpenter, A. E. et al. CellProfiler: image analysis software for identifying and quantifying cell phenotypes. *Genome Biol.* **7**, R100 (2006).
- Dobin, A. et al. STAR: ultrafast universal RNA-seq aligner. *Bioinformatics* **29**, 15–21 (2013).
- Anders, S., Pyl, P. T. & Huber, W. HTSeq—a Python framework to work with high-throughput sequencing data. *Bioinformatics* **31**, 166–169 (2015).
- McCarthy, D. J., Chen, Y. & Smyth, G. K. Differential expression analysis of multifactor RNA-seq experiments with respect to biological variation. *Nucleic Acids Res.* **40**, 4288–4297 (2012).

### Acknowledgements

We thank F. Ringnalda for the initial establishment of colon organoid cultures in the Schwank laboratory; G. Rogler, B. Morell and M. Scharl for providing intestinal rest material; S. Allazetta for providing PEG hydrogel microbeads; N. Landwehr for help with video production; and M. Leleu for the bioinformatics analysis. Intestinal tissue samples were obtained from the Department of Gastroenterology and Hepatology, University Hospital Zürich under ethical approval from the Cantonal Ethics Committee of the Canton Zürich, Switzerland (EK-1755). Colorectal tumour samples were obtained from the Department of Gastroenterology and Hepatology, Centre Hospitalier Universitaire Vaudois under ethical approval from the Cantonal Ethics Committee of the Canton Vaud, Switzerland (CER-VD: 2017-00359). This research was funded by the project 'OPERON' from the Personalized Health and Related Technologies Initiative from the ETH Board, as well as École Polytechnique Fédérale de Lausanne (EPFL).

### Author contributions

N.B., S.H. and M.P.L. conceived the study, designed experiments, analysed data and wrote the manuscript. F.K. and G.T. helped to design the screening experiments and analysed the data. K.H. designed the drug panel and gave valuable feedback on experimental designs. C.C. helped conduct mouse intestinal organoid experiments. N.G., T.R. and G.S. gave feedback on experimental designs. T.R. and G.S. helped to design experiments and analysed data with human cells. F.K., K.H., N.G., T.R., G.S. and G.C. provided inputs on the manuscript.

### Competing interests

The Ecole Polytechnique Fédérale de Lausanne has filed for patent protection on the technology described herein (PCT/IB2014/067242, published as CA2972057A1, CN107257850A, EP3237597A1, WO2016103002A1 JP2018504103A and US2018264465A1; and PCT/EP2017/073357, published as EP3296018A1, EP3515600A1, WO2018050862A1 and US2020010797A1), and S.H., N.B., N.G. and M.P.L. are named as inventors on those patents; S.H., N.B. and M.P.L. are shareholders in SUN bioscience SA, which is commercializing those patents.

### Additional information

**Supplementary information** is available for this paper at <https://doi.org/10.1038/s41551-020-0565-2>.

**Correspondence and requests for materials** should be addressed to M.P.L.

**Reprints and permissions information** is available at [www.nature.com/reprints](http://www.nature.com/reprints).

**Publisher's note** Springer Nature remains neutral with regard to jurisdictional claims in published maps and institutional affiliations.

© The Author(s), under exclusive licence to Springer Nature Limited 2020

## Reporting Summary

Nature Research wishes to improve the reproducibility of the work that we publish. This form provides structure for consistency and transparency in reporting. For further information on Nature Research policies, see [Authors & Referees](#) and the [Editorial Policy Checklist](#).

### Statistics

For all statistical analyses, confirm that the following items are present in the figure legend, table legend, main text, or Methods section.

- | n/a                                 | Confirmed  |
|-------------------------------------|--|
| <input type="checkbox"/>            | <input checked="" type="checkbox"/> The exact sample size ( $n$ ) for each experimental group/condition, given as a discrete number and unit of measurement  |
| <input type="checkbox"/>            | <input checked="" type="checkbox"/> A statement on whether measurements were taken from distinct samples or whether the same sample was measured repeatedly  |
| <input type="checkbox"/>            | <input checked="" type="checkbox"/> The statistical test(s) used AND whether they are one- or two-sided<br><i>Only common tests should be described solely by name; describe more complex techniques in the Methods section.</i>   |
| <input checked="" type="checkbox"/> | <input type="checkbox"/> A description of all covariates tested  |
| <input type="checkbox"/>            | <input checked="" type="checkbox"/> A description of any assumptions or corrections, such as tests of normality and adjustment for multiple comparisons  |
| <input type="checkbox"/>            | <input checked="" type="checkbox"/> A full description of the statistical parameters including central tendency (e.g. means) or other basic estimates (e.g. regression coefficient) AND variation (e.g. standard deviation) or associated estimates of uncertainty (e.g. confidence intervals) |
| <input type="checkbox"/>            | <input checked="" type="checkbox"/> For null hypothesis testing, the test statistic (e.g. $F$ , $t$ , $r$ ) with confidence intervals, effect sizes, degrees of freedom and $P$ value noted<br><i>Give <math>P</math> values as exact values whenever suitable.</i>                            |
| <input checked="" type="checkbox"/> | <input type="checkbox"/> For Bayesian analysis, information on the choice of priors and Markov chain Monte Carlo settings  |
| <input type="checkbox"/>            | <input checked="" type="checkbox"/> For hierarchical and complex designs, identification of the appropriate level for tests and full reporting of outcomes   |
| <input type="checkbox"/>            | <input checked="" type="checkbox"/> Estimates of effect sizes (e.g. Cohen's $d$ , Pearson's $r$ ), indicating how they were calculated   |

*Our web collection on [statistics for biologists](#) contains articles on many of the points above.*

### Software and code

Policy information about [availability of computer code](#)

#### Data collection

Nikon Ti Control software (Nikon) was used to acquire all wide-field images.  
ZEN 2010B SP1 (Zeiss) was used to acquire images from a Zeiss LSM700 Confocal microscope.  
An IN Cell Analyzer 2200 (GE Healthcare) was used to acquire all images of the drug-screening experiments.

#### Data analysis

Fiji-ImageJ (v 2.0.0-rc-69/1.52p) was used to process images and to extract quantitative data for the analysis.  
Prism 8 (Graphpad Softwares) was used for data representation and statistical analyses.  
CellProfiler software 3.1.8 was used to process all images and to extract data from the drug-screening experiments.  
Knime (<https://www.knime.com/>) was used to process and perform the statistical analyses of all data extracted from CellProfiler.  
R Version 3.2.2 and the edgeR package were used to process the bulk RNAseq dataset.  
The gene-ontology analysis was performed by using the online tool string-db.org, and the Venne diagram was generated using the online tool [bioinformatics.psb.ugent.be/webtools/Venn/](http://bioinformatics.psb.ugent.be/webtools/Venn/).

For manuscripts utilizing custom algorithms or software that are central to the research but not yet described in published literature, software must be made available to editors/reviewers. We strongly encourage code deposition in a community repository (e.g. GitHub). See the Nature Research [guidelines for submitting code & software](#) for further information.

### Data

Policy information about [availability of data](#)

All manuscripts must include a [data availability statement](#). This statement should provide the following information, where applicable:

- Accession codes, unique identifiers, or web links for publicly available datasets
- A list of figures that have associated raw data
- A description of any restrictions on data availability

The main data supporting the results in this study are available within the paper and its Supplementary Information. The raw and analysed datasets generated during the study are too large to be publicly shared, yet they are available for research purposes from the corresponding authors on reasonable request. The RNA

## Field-specific reporting

Please select the one below that is the best fit for your research. If you are not sure, read the appropriate sections before making your selection.

Life sciences  Behavioural & social sciences  Ecological, evolutionary & environmental sciences

For a reference copy of the document with all sections, see [nature.com/documents/nr-reporting-summary-flat.pdf](https://www.nature.com/documents/nr-reporting-summary-flat.pdf)

## Life sciences study design

All studies must disclose on these points even when the disclosure is negative.

Sample size	We considered that three technical replicates per biological repeat and three biological repeats were sufficient to understand the reproducibility of our results.
Data exclusions	No data acquired for quantitative analysis were excluded.
Replication	The vast majority of the conditions have been independently experimentally repeated a minimum of three times, some of them (as indicated in the manuscript) have been independently experimentally repeated two times. In all the attempts at repetition for each specific condition we observed similar behavior.
Randomization	Not relevant to this study.
Blinding	Not relevant to this study.

## Reporting for specific materials, systems and methods

We require information from authors about some types of materials, experimental systems and methods used in many studies. Here, indicate whether each material, system or method listed is relevant to your study. If you are not sure if a list item applies to your research, read the appropriate section before selecting a response.

### Materials & experimental systems

n/a	Involved in the study
<input type="checkbox"/>	<input checked="" type="checkbox"/> Antibodies
<input type="checkbox"/>	<input checked="" type="checkbox"/> Eukaryotic cell lines
<input checked="" type="checkbox"/>	<input type="checkbox"/> Palaeontology
<input checked="" type="checkbox"/>	<input type="checkbox"/> Animals and other organisms
<input checked="" type="checkbox"/>	<input type="checkbox"/> Human research participants
<input checked="" type="checkbox"/>	<input type="checkbox"/> Clinical data

### Methods

n/a	Involved in the study
<input checked="" type="checkbox"/>	<input type="checkbox"/> ChIP-seq
<input checked="" type="checkbox"/>	<input type="checkbox"/> Flow cytometry
<input checked="" type="checkbox"/>	<input type="checkbox"/> MRI-based neuroimaging

## Antibodies

Antibodies used	Primary antibodies: L-FABP (host: rabbit, dilution 1:50, Santa Cruz sc-50380), lysozyme (host: rabbit, dilution 1:50, Thermo Scientific PA1-29680), chromogranin-A (host: rabbit, dilution 1:50, Santa Cruz sc-13090), Mucin-2 (host: rabbit, dilution 1:50, Santa Cruz sc-15334) and SOX-9 (host: rabbit, dilution 1:50, ab185966). Secondary antibody: Alexa 647 goat- $\alpha$ -rabbit (dilution 1:1000; Invitrogen), Phalloidin (dilution 1:200, Life Technologies) and DAPI (dilution: 1:1000, Sigma).
Validation	The antibodies were tested on differentiated LGR5:GFP mouse intestinal organoids following published protocols of differentiation. In the immunofluorescence procedure a "No Primary Control sample" was used as reference for the background signal.

## Eukaryotic cell lines

Policy information about [cell lines](#)

Cell line source(s)	LGR5-eGFP reporter mouse intestinal stem cells were extracted from the small intestines of LGR5-eGFP reporter mice following published protocols. Human colon organoids were obtained by extracting crypts from colon biopsies obtained from the Department of Gastroenterology and Hepatology, University Hospital Zürich, under ethical approval from the Cantonal Ethics Committee of
---------------------	---

	<p>the Canton Zürich, Switzerland (EK-1755). Human iPS cell-derived intestinal organoids were obtained from Prof. Kim Jensen (BRIC, University of Copenhagen, Copenhagen, Denmark). Colorectal cancer organoids were obtained by dissociating and culturing colorectal tumour samples obtained from the Department of Gastroenterology and Hepatology, Centre Hospitalier Universitaire Vaudois, under ethical approval from the Cantonal Ethics Committee of the Canton Vaud, Switzerland (CER-VD: 2017-00359). HCT116 (human colorectal carcinoma) cell line was purchased from ATCC.</p>
Authentication	<p>The human colon organoids as well as the human colorectal organoids were authenticated at the time of extraction. The human iPS-cell-derived intestinal organoid line has been authenticated in the laboratory from which the cells were received. HCT116 cells were authenticated at the time of purchase.</p>
Mycoplasma contamination	<p>All the cell lines used in this work have been routinely tested for mycoplasma infection, with negative results.</p>
Commonly misidentified lines (See <a href="#">ICLAC</a> register)	<p>None of the cell lines used in this study are present in the ICLAC register.</p>